Monitoring of earth concrete damage evolution during drying

Nathalie Kouta, Jacqueline Saliba, Nadia Saiyouri

Monitoring of earth concrete damage evolution during drying

Nathalie Kouta, Jacqueline Saliba, Nadia Saiyouri

Université de Bordeaux, UMR 5295, Institut de Mécanique et d'Ingénierie (I2M), CNRS, Esplanade des Arts et Métiers, 33405 Talence, France.

Abstract. Earth concrete, constituted mainly of raw earth, is a promising ecofriendly material for future constructions. However, it is composed of fine particles like clay which make it very sensitive to drying. The volume change induced by desiccation shrinkage can be responsible of cracking which can have a detrimental effect on the durability and mechanical properties. Thus, in order to design reliable earth concrete structures, considering a coupling between drying shrinkage and damage is important. The effect of curing conditions on the mechanical properties of earth concrete with different percentages of flax fibers has been studied. The evolution of damage during drying has been monitored continuously using the ultrasound and the acoustic emission (AE) techniques. The mechanical properties of earth concrete decreases for specimens stored at low relative humidity. In addition, the AE results associated with shrinkage and mass loss measurement made it possible to describe qualitatively the drying process.

Keywords: earth concrete, shrinkage, drying, damage, Acoustic Emission technique.

1. Introduction

Over the past decade, a large amount of natural resources has been consumed by the construction sector accompanied with the emission of a large amount of CO_2 due to the production of cement. Hence, due the increase awareness, many studies are now conducted to find an alternative ecofriendly material. In the case of structures that do not require high mechanical performance, earth concrete can be considered as an acceptable solution in comparison to conventional concrete [1]. In addition, this latter presents many advantages in terms of hygrothermal and acoustical performance [2].

However, the presence of a large quantity of fine particles in earth concrete makes it very sensitive to different types of shrinkage which can induce cracking and affect its strength and durability [3–5].

Earth concrete volume change is an unavoidable phenomenon, from very early age to long-term behavior. At early age (before 24 h), earth concrete goes through negative volumetric variations due to water evaporation (plastic shrinkage) or internal reactions of chemical origins (autogenous shrinkage) linked to the hydration of binders. The menisci present at the interface between the water-filled and empty pores will result in the development of stresses within the liquid phase. These stresses pull earth concrete matrix particles closer together and lead to a volume reduction and strains within the solid framework. The autogenous shrinkage component, being mainly dependent on the composition of earth concrete, develops more rapidly with time than drying shrinkage. Long term drying shrinkage (after 24 h) depends on the age at the beginning of drying and external parameters such as relative humidity (RH) and specimen size [6]. The shrinkage of different types of earth construction have been studied in the literature [7,8]. [9] studied drying shrinkage for un-stabilized rammed earth walls. Volumetric shrinkage developed in the two direction of the wall with a value that do not exceed 5%. This value depends on clay content, grain size of the soil and drying rate and process that is related to the radius of the pores. Shrinkage of rammed earth is much higher than that of conventional concrete, with a faster evolution in the initial phase, representing 85% of the total shrinkage recorded during the first 28 days [10]. In addition, specimens stored at a RH of 95% have a total shrinkage 20% lower than specimens stored at a RH of 35%. Drying shrinkage for cement-stabilized soils is mainly related to the plasticity index of the soil, the clay content [11] and the clay minerals present in the soil [12]. Increasing clay content increases desiccation shrinkage [13]. If tensile strength is less than stress induced by shrinkage restraint , cracking will occur in earth concrete [6]. Micro cracking during shrinkage depends on the type of restraint which can be caused by the structure (externally applied restraint) or the material (internal restraint). Self-restraining mechanisms can be related to moisture/shrinkage gradients that develop at different depths in the specimens and by the presence of aggregates. Those micro cracks increase the permeability of earth concrete and can lead to stress concentrations during loading. Earth concrete structures are therefore vulnerable to inherent stresses or shrinkage-induced cracks that can not only cause structural defects, but also reduce the

55 serviceability, durability and aesthetics of earth concrete [14]. Carbonation reactions also occur in the
56 long term due to the penetration of carbon dioxide into earth concrete, leading to the formation of
57 calcite [15]. Carbonate crystals have weak cohesion properties and the presence of calcite does not
58 really improve the mechanical performance of earth concrete [16].

59 Early age shrinkage or plastic shrinkage of earth concrete has been studied in a previous study
60 [3] and more particularly the effect of flax fibers on cracking sensitivity. In fact, fibers have been
61 widely used for soil reinforcement and to reduce cracking induced by plastic shrinkage in concrete at
62 early age [3]. Vegetable fibers have the advantage of being light, ecological, with low-cost as they are
63 produced as waste materials, in addition to their good acoustic and hygrothermal properties and
64 compatibility with earth concrete. [3,17] showed that flax fibers enhanced the ductility of earth concrete
65 by generating a diffused cracking and decreased the horizontal plastic shrinkage. Thus, flax fibers
66 reduce the cracking risk of restrained earth concrete at early age [3]. The use of natural fibers can be
67 sensitive in the long term due to their natural decomposition and biological attack [18]. High humidity
68 can promote this kind of activity within the material and accelerate the biodegradation [19]. Soil
69 stabilization increases the resistance to biological attacks [20]. Shrinkage is also influenced by the
70 fiber's type and content [21]. The rate of shrinkage increases with clay and water content but decreases
71 with fiber content [22]. The addition of fibers improves also the strength and reduces shrinkage
72 cracking of earth concrete [22,23]. The stabilization of shrinkage occurred earlier with adding straw,
73 indicating a rapid drying due to the accelerated evaporation through the air channels formed [23]. The
74 addition of 4% of sisal or coconut fibers reduced tensile shrinkage cracking [24].

75 In this study, long-term shrinkage and the effect of drying on the mechanical properties of earth
76 concrete have been investigated.

77 In order to monitor damage evolution during shrinkage, the AE technique has been used. This
78 technique has been widely used to monitor damage and crack development during mechanical loading
79 [25–29]. Recently, it has been also used to understand some complex phenomena as corrosion [30],
80 creep [31], hardening of cement paste and concrete [32], drying shrinkage cracking in cement-based
81 materials [33–36] and drying of ceramics [32]. Different mechanisms have been proposed to explain
82 the reasons behind the AE activity during the cement paste hydration as the formation and dissolution

of hydrates, the consumption of water and the emptying of capillary pores [32]. [37] attributed the AE activity during self-desiccation to cavitation.

A comprehensive study of the damage process during shrinkage of earth concrete is proposed in this paper using the AE technique. First, the materials and the experimental methods are presented. Then, desiccation shrinkage and its effect on the mechanical properties are analyzed. Finally, the characterization of damage evolution under drying is suggested using the AE method.

2. Experimental program

2.1 Materials

2.1.1. *Soil and Hydraulic binders*

The soil of earth concrete mixtures is based on an artificial soil composed of 30% of bentonite clay (75% of Smectite, 15% of Illite and 10% of Kaolinite) and 70% of sand [3]. This artificial soil has been chosen in order to avoid the variability of onsite soil. The artificial soil has been stabilized with 3% of natural hydraulic lime (NHL5/ EN 459-1 [38]) and 8% of cement (CEM 1, 52.5 N PM-CP2 / EN197-1 [39]) based on the clay and sand mixture mass. Those percentages have been fixed according to other studies presented in the literature that showed that 2% to 4% of lime are sufficient to stabilize the soil [40,41], and the optimal percentage of cement to ensure a sufficient strength for earth concrete is 8% [42]. The pure Portland cement CEM 1 composed mainly of clinker is chosen to prevent the effect of additional components.

2.1.2. *Flax fibers*

Flax fibers are natural fibers, bio-renewable, recyclable and biodegradable. The fibers were cut at constant length of 12 mm and their diameter is equal to 14.66 µm ±2.95 [43]. These fibers are rich in cellulose, more than 60% of their constitution, which gives them good tensile strength [44]. The fibers used in this study were not treated in order to keep them natural and easy to use.

2.2 Mixtures

Three mixtures have been tested by varying the percentage of flax fibers: 0, 0.3 and 0.6%. Clay and sand were first mixed during 3 minutes to homogenize of the artificial soil. Then, lime and cement were added to the dry mixture and mixed during 2 minutes. Water and superplasticizer were then added and mixed for 3 minutes. The superplasticizer Tempo 10 has been used due to its efficiency as a water reducer admixture in earth concrete [8]. Finally, fibers were progressively added and mixed during 3 minutes. Table 1 presents the mixtures components and composition. The quantity of fibers was subtracted from the artificial soil mass to keep an equivalent solid mass. The effective water to binder ratio was kept constant and equal to 0.45. Additional water has been added to take into account water absorbed by flax fibers. Details about the constituents and mixture properties at early age can be found in [3].

Table 1. Mixtures components and composition.

Components (kg/m^3)	Sand	Bentonite	Cement	Lime	Total water	Super-plasticizer	Flax fibers
SA0F	931	405	152	34.2	367	1.6	0
SA03F	929	401	152	34.2	370	1.6	5.7
SA06F	925	399	152	34.2	375	1.6	11.4

3. Methods

3.1 Compressive test

Unconfined compressive tests have been conducted using an electromechanical machine with a capacity of 100 kN (**Figure 1**). A constant loading displacement rate of 0.6 mm/min has been considered. This test has been realized on cubic specimens of 10×10×10 cm^3 at the age of 28 and 180 days. After pouring earth concrete, specimens were covered with a thin sheet of plastic in order to prevent water loss and maintained at a temperature of 20°C during 48 h. Then, specimens were unmolded and stored in two different curing conditions at a RH of 90% and 50% (± 5%) and a temperature of 20 °C.

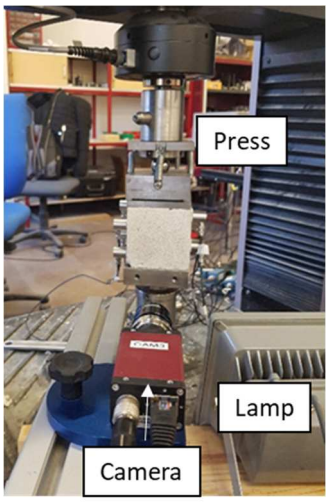

Figure 1. Compressive test set up

3.2 Ultrasound test

The ultrasound system PUNDIT (Portable Ultrasonic Nondestructive Digital Indicating Tester) was used to measure the velocity of ultrasound waves. It consists of a pulse generator with two transducers. An electrical pulse is converted into a longitudinal pressure wave with a frequency of 200 kHz by using a transmitter coupled to the surface with grease.

3.3 Digital image correlation technique

The compressive tests were monitored with the digital image correlation (DIC) technique. It is a direct and simple method for fracture examination. The usage of this technique implicates an advance surface preparation of earth concrete specimens by using a white and black speckle (white paint at the bottom with small black dots above). The displacement of the tested surface of the specimen is obtained by the analysis of the random speckle at different instances based on the pictures taken during the test. The photos of the specimen's surface have been captured using a digital camera. The reference images have a resolution of 2452 × 2056 pixels. To improve the luminosity of the photos, two lamps have been used in parallel. Images have been taken at a rate of one image per second during the tests and stored

152 directly. The treatment of the images has been realized using the commercial software Vic 2D with a
153 resolution of 0.05 mm per pixel.
154

155 ### 3.4 Shrinkage and water loss measurement tests

156 Shrinkage tests were carried out on prismatic specimens of 7x7x28 cm^3 fitted with metal studs
157 at their ends. Specimens were poured and kept for 24 hours in sealed conditions to avoid drying. After
158 24 hours, specimens were removed from the molds and shrinkage tests were carried out in an air-
159 conditioned room at 20 °C (± 2 °C) and a RH of 50% (± 5%). The measurement of the longitudinal
160 deformation was carried out using LVDT sensors with a precision of 3 µm during several weeks. For
161 total shrinkage, the ends of the specimens were covered with an adhesive aluminum tape to allow
162 identical lateral drying of the four sides of earth concrete. For Autogenous shrinkage, specimens were
163 completely covered with two layers of adhesive aluminum tape to prevent drying. The mass loss was
164 measured simultaneously on specimens with the same dimensions and stored under the same drying
165 conditions.
166

167 ### 3.5 Acoustic Emission technique

168 The AE method was used to monitor the damage evolution in earth concrete specimens during
169 shrinkage. The AE system comprised of an eight channel AE Win system, a general-purpose interface
170 bus (2PCI-DISP4) and a PC for data storage analysis. Four piezoelectric transducers with a resonant
171 frequency of 150 KHz were used to convert the mechanical waves to electrical signals (**Figure 2**). They
172 were placed on specimens using silicon grease as a coupling agent. The recorded AE amplitudes range
173 from 0 to 100 dB. The detected signals are amplified with a 40 dB gain differential amplifier. The
174 signal detection threshold is set at a value of about 35 dB to overcome the background noise (RILEM
175 TC212-ACD). The acquisition parameters are set as follows: peak definition time (PDT) = 100 µs, hit
176 definition time (HDT) = 200 µs and hit lock time (HLT) = 400 µs. A high pass filter with a cut-off
177 frequency of 20 KHz, and a low-pass filter with a cut-off frequency of 400 KHz are used to eliminate

mechanical and electro-magnetic disturbances. Several signal descriptors were calculated by AEwin system.

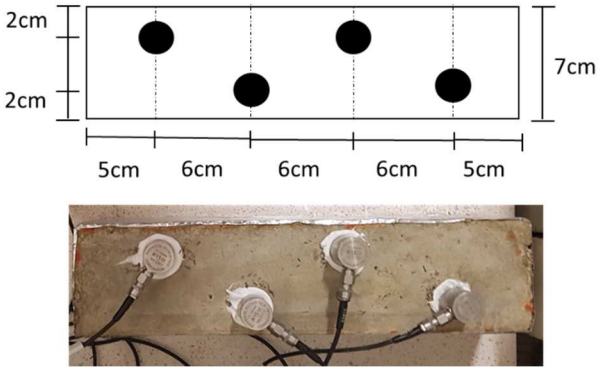

Figure 2. Prismatic specimen geometry and position of AE transducers

4. Results

4.1 Mechanical properties

Figure 3 shows the stress/strain curves for specimens conserved at two different conditions at the age of 28 and 180 days. The strain was calculated as the ratio between the average displacement, obtained using the digital image correlation, and the length of the specimen. In fact, the press displacement does not reflect the real deformation of earth concrete specimens. The deformation calculated from the press displacement is higher than that of DIC due to the deformation of the frame and the crushing of concrete at the contact between the metallic plates and concrete specimen. Different phases can be distinguished. For mixtures stored at 90% of RH, the stress increased linearly in function of the strain almost till the maximal strength showing an important elastic phase. However, for specimens stored at 50% of RH, the elastic phase was observed. The slope of the elastic phase decreases with an important rate as RH decreases while the strain at the peak increases. After the peak, the load decreases quickly for SA0F indicating a brittle behavior of earth concrete conserved at 90% of RH in comparison to that stored at 50% of RH. For specimens with fibers, the post peak region zone was

more important indicating an increase of earth concrete ductility due to different softening mechanisms [19].

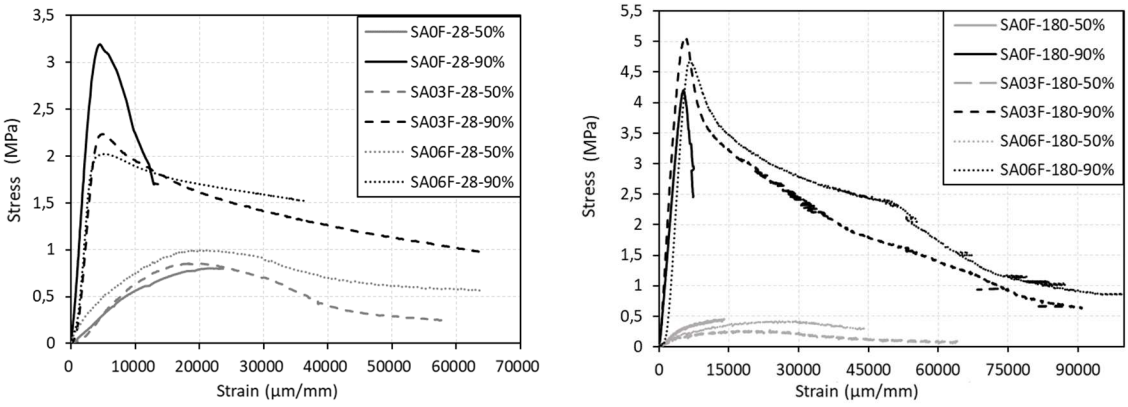

Figure 3. Stress-strain curves of earth concrete specimens conserved at 50% and 90% of RH for SA0F, SA03F and SA06F at the age of 28 days (a) and 180 days (b)

Figure 4 shows the maximum compressive stress and the elastic modulus of earth concrete specimens kept at 90% and 50% RH at the age of 28 and 180 days. For the mixtures kept at 90% of RH, the compressive strength decreases slightly with the addition of fibers at the age of 28 days which may be due to the higher porosity [3]. The compressive strength of earth concrete increased with age specially for specimens with fibers which may be due to time-dependent pozzolanic reactions [40]. In fact, the formed hydrates bind the soil particles together and give them a more compact matrix structure. This limits considerably the particles rearrangement at the interface and increases the effective interfacial contact area. In addition, as natural fibers are characterized by their hydrophilicity, hydrates may cover the surface of fibers due to the presence of water and improve the characteristics of the interfacial bonding and the frictional force between the fibers and the matrix [45,46].

For specimens kept at 50% of RH, a high reduction of strength has been observed due to drying with a slight effect of the percentage of fibers. This reduction of strength continues with the age of curing at 180 days.

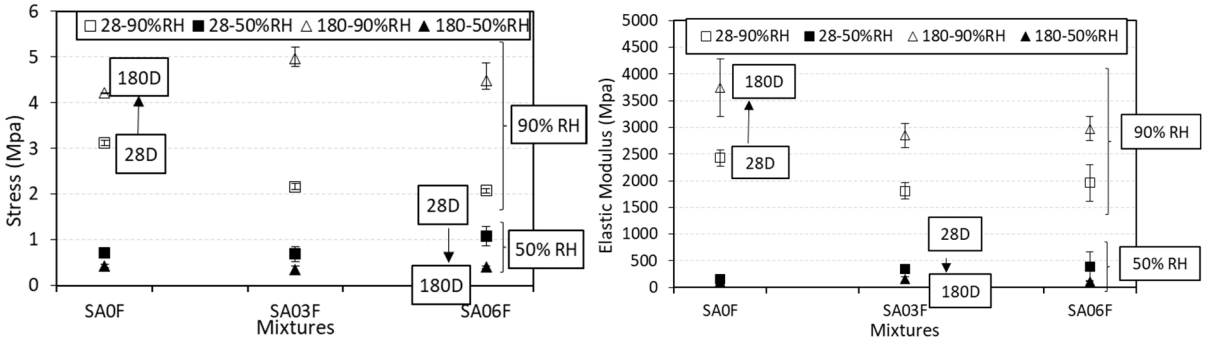

Figure 4. Maximum strength and Young modulus of SA0F, SA03F and SA06F conserved at 50% and 90% of RH at the age of 28 and 180 days.

The decrease of the mechanical properties of earth concrete specimens may be due to degradation induced by desiccation shrinkage. This degradation can be observed visually at the surface of the specimens (**Figure 5**). The photos were taken before the compression test at the age of 180 days for specimens stored at 50% of RH. The photos show the flaking of the surface especially for specimens without fibers in addition to visible cracks. Cracks were detected at the 28th day for SA0F and spread rapidly over the entire surface of earth concrete, inducing a progressive loss of the surface layer. In fact, micro cracks may develop in earth concrete due to gradient deformation during drying, in addition to the decrease of hydration reactions and the loss of the cohesion between the particles. For the mixtures with fibers, cracks were more visible at the 180th day, without leading to a significant loss of earth concrete surface. This slower degradation may be associated to a better crack resistance. In fact, the presence of fibers may prevent the propagation of cracks due to the adhesion between the matrix and the fibers and the bridging effect [47,48]. However, this adhesion may decrease during the drying process due the strain gradient at the interface between the matrix and the fibers which may be responsible of the lower strength at the 180th day. This may be also due to a different pore size distribution that can modify the capillary pressure and thus the stress gradient that may impact the mechanical and transfer properties of earth concrete.

Figure 5. Photos of SA0F, SA03F and SA06F before the compression test at 50% of RH at the age of 180 days

4.2 Digital image correlation monitoring of fracture tests

For a better understanding of the fracturing process, the compressive tests were monitored with the DIC method. **Figure 6** presents the 2D strain fields along the X direction for SA0F, SA03F and SA06F stored at 50% and 90% of RH at different loading levels. For specimens kept at 90% of RH, no cracks have been visualized in the elastic phase and macro cracks started to propagate slightly before the peak. For SA0F, a large crack has been observed with an important width. The developed cracks led to the loss of strength and the total rupture of SA0F at 50% of the maximum strength in the post peak region. The rupture type shows clearly a lateral confinement. In fact, due to friction, a triaxial stress state was created within the material in the areas near the loading plates. Vertical cracks appeared mainly near the corners of the lateral surface and were coupled with the horizontal ones due to bending [49]. Consequently, a big part of the specimen fell indicating a brittle fracture of the specimen [23].

However, for specimens with fibers, a diffuse multi cracking has been observed at the peak with small crack openings. This indicates a more ductile behavior due the presence of fibers that limit the crack propagation and opening by bridging the cracks and redistributing the applied stress during the extension [19,23,49]. Additional cracks have been observed in the post peak region and crack openings increased at the surface with no clear effect of the lateral confinement. This multi cracking is partially responsible of the higher fracture energy and ductility of the material [50].

For specimens stored at 50% of RH, cracks appeared earlier at 50% of the maximum strength for SA0F and 80% of the maximum strength for mixtures with fibers. This confirms the degradation of earth concrete specimens and the pre-presence of micro cracks that developed during drying [8]. Several cracks were observed for SA0F. The crack openings were also more important for SA0F indicating the effect of fibers in increasing the ductility and preventing the brittle rupture.

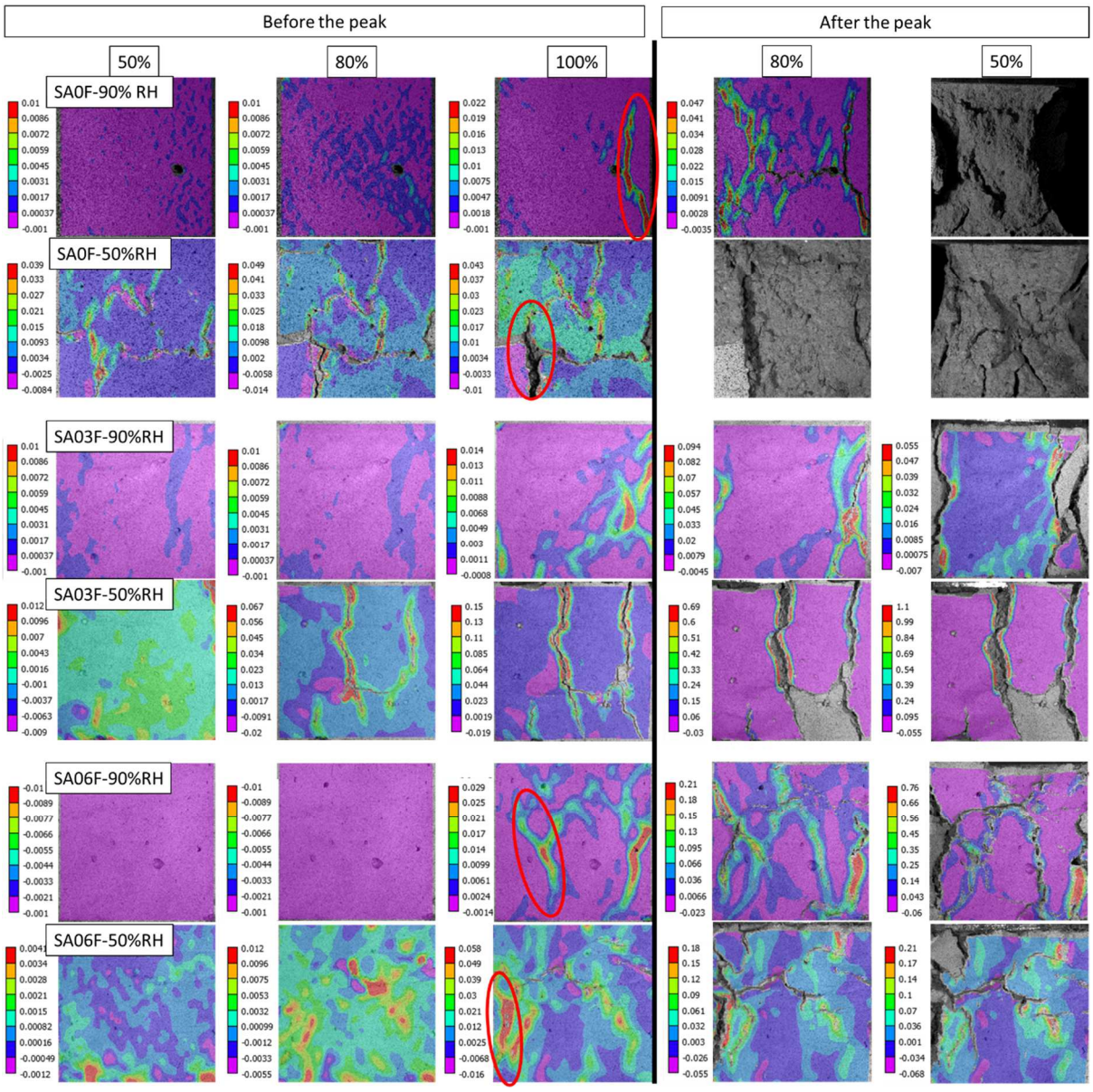

Figure 6. 2D strain fields along X for SA0F, SA03F and SA06F stored at 50% and 90% of RH at different loading levels.

Figure 7 presents the evolution of a chosen crack width (circled in figure 8) along the height of specimens SA0F and SA06F at 50% and 90% of RH. The crack width increases with the applied load. It started earlier for specimens kept at 50% of RH at 30% of the maximum strength for SA0F and 80% of the maximum strength for SA06F which confirms the pre-cracking of specimens subjected to drying. In addition, the width of the cracks was much larger for specimens kept at 50% of RH than that kept at 90% of RH for the different loading levels. Note that the crack width varied along the crack length due to different stress gradient in addition to the effect of flax fibers distribution and orientation. The addition of flax fibers slowed down crack openings and increased earth concrete ductility. In fact, flax fibers held the soil matrix together by bridging the cracks, in addition to stress transfer and redistribution in earth concrete [24]. The good adhesion between fibers and earth concrete matrix prevented the spread of large crack opening and improved the fracture energy. The rupture occurred due to the debonding of flax fibers from the matrix.

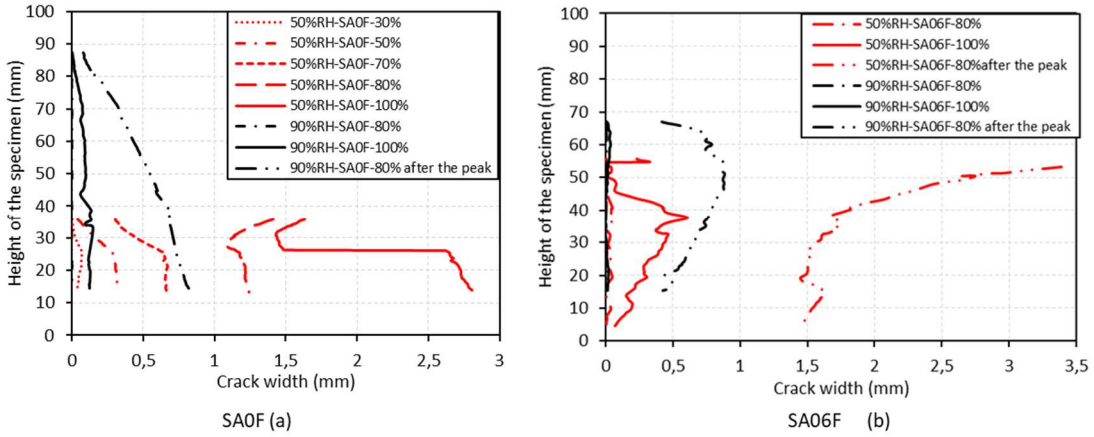

Figure 7. Evolution of the crack width for (a) SA0F and (b) SA06F at 50% and 90% of RH

To gain a better understanding of the effect of drying, long term shrinkage was evaluated and specimens were monitored with the ultrasound and the AE techniques.

290 ### 4.3 Long term shrinkage

291 To improve the comprehension of the different mechanisms responsible of the degradation of
292 the mechanical properties of earth concrete due to drying, the evolution of shrinkage in correlation with
293 the mass loss has been studied. **Figure 8** (a) presents the evolution of the total shrinkage, autogenous
294 shrinkage and weight loss of SA0F and SA06F in function of time. Autogenous shrinkage occurs
295 independently of the external water loss and is a result of chemical shrinkage and self-drying shrinkage.
296 The autogenous shrinkage of earth concrete with and without fibers increases slightly in the first 3 days
297 after casting and then stabilized. Desiccation shrinkage occurs in earth concrete due to self-desiccation
298 (internal drying) and mainly due to the loss of water from capillary pores and the gel (external drying).
299 Total shrinkage is therefore represented as the sum of desiccation and autogenous shrinkage. The
300 reduction of RH in the pore system causes a water–air meniscus that subjects the pore walls to
301 considerable stress and leads to substantial drying shrinkage. The shrinkage rate is slow during the first
302 three days after casting. Then, it increases with an important rate and begins to decrease gradually in
303 function of time to stabilize after 20 days. Desiccation shrinkage is almost 10 times higher than
304 autogenous shrinkage. Note that drying shrinkage values are very important in comparison to ordinary
305 concrete which may be due to a higher capillary pressure and a less rigid solid skeleton.[14].

306 The evolution of desiccation shrinkage in function of the weight loss has been also plotted and
307 shows two phases (**Figure 8** (b)). During the first 3 days after casting, even though the weight loss rate
308 is important (about 7%), the generated shrinkage is low. In the second phase, the weight loss and
309 desiccation shrinkage with increased with an important rate proportionally. The slope variation can be
310 explained by the modification of the dimension of the pores that are being emptied and the decrease of
311 the evaporation rate. In fact, during the drying process some of the liquid water cannot reach the surface
312 and evaporates within the pores.

313

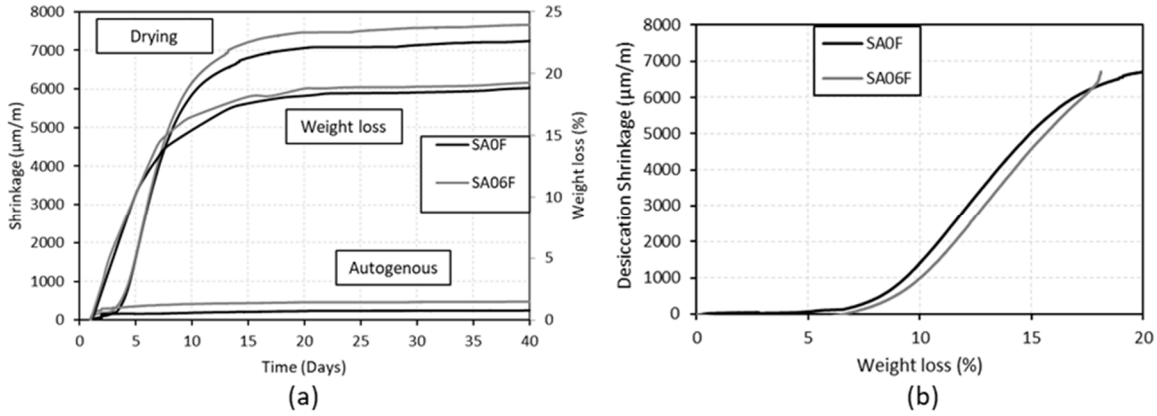

Figure 8. (a) Evolution of total shrinkage, autogenous shrinkage and weight loss in function of time and (b) evolution of desiccation shrinkage in function of the weight loss for SA0F and SA06F

The same behavior has been observed for mixtures with and without fibers. From the beginning of the test and till the 6th day after casting, the weight loss and shrinkage were the same for the two mixtures. However, after this age, the weight loss and the total shrinkage increase slightly for mixtures with fibers. This may be due to the higher water absorption with fibers.

4.4 Ultrasound monitoring

Figure 9 shows the comparison between the ultrasonic waves propagation velocity of specimens kept at 50% and 90% of RH in function of the curing age. For specimens kept at 90% of RH, the velocity increases with an important rate during the first days and slightly after the age of 28 days indicating the increase of stiffness [51]. For specimens kept at 50% of RH, the wave propagation velocity is smaller. It increases during the first days but the velocity measurement becomes impossible after 8 days for SA03F and 12 days for SA06F. This can be related to water loss and premature damage of specimens due to drying that may cause cracking and a loss of cohesiveness between particles [52].

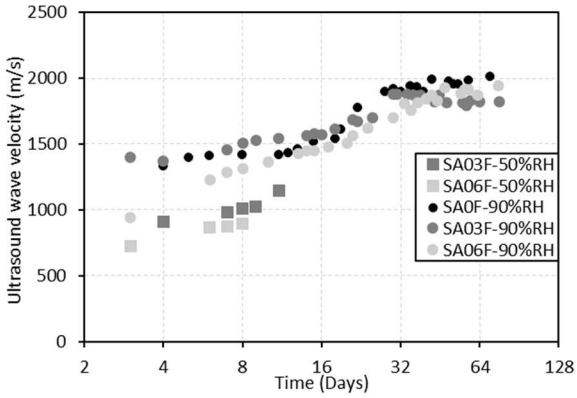

Figure 9. Evolution of the ultrasonic wave velocity at 50% and 90% of RH in function of time.

For a better understanding of the different phenomena occurring during drying, shrinkage tests have been also monitored using the AE technique.

4.5 AE monitoring of drying tests

AE hits provide an indication on the number of burst emissions and wave characteristics, such as the amplitude, duration and absolute energy. The AE hits detected during shrinkage may be generated due to micro cracking or cavitation [37]. In fact, when evaporation occurs at the surface of the pore, the radius of the liquid/vapor interface or meniscus decreases. When the radius of curvature of the meniscus is small, it retreats into the pore and produces a kinetic energy generating the propagation of mechanic waves [53]. Micro cracks can be generated due to moisture gradient that leads to non-uniform drying shrinkage. As the surface of the material exposed to drying shrinks faster, micro cracks are mainly generated at the surface [54]. Shrinkage can be also restrained by the presence of aggregates or fibers inducing micro cracking at the interface with the matrix [55].

Figure 10 shows the cumulated number of AE hits in correlation with shrinkage in function of time. For a better analysis, the cumulative number of AE hits has been also plotted in function shrinkage for SA0F and SA06F. Three phases similar to those observed while plotting the relationship between the weight loss and shrinkage have been obtained. During the first phase, few AE hits were detected. They reached a value of 500 for a shrinkage value equal to 3200 µm/m. This phase is mainly related to the departure of water from the surface and larger porosity. The numbers of AE hits was similar for

both mixtures. During the second phase between the 6th and the 11th day after pouring, the number of the cumulative number of AE hits increases with an important rate (from 500 to 4000 signals). This may be related to micro cracks generated by non-uniform desiccation shrinkage at the surfaces exposed to drying. This can be also the reason behind the inability to measure the ultrasonic velocity for SA06F12 after the 11th day (**Figure 6**). The cumulative number of AE hits was more important for SA0F for the same level of shrinkage indicating a higher damage level. This is confirmed with the compressive tests where the decrease of strength was more important for SA0F. During the third phase, a notable decrease in the acoustic activity was observed indicating the decrease of micro cracks generation in parallel with the decrease of the weight loss and shrinkage stabilization.

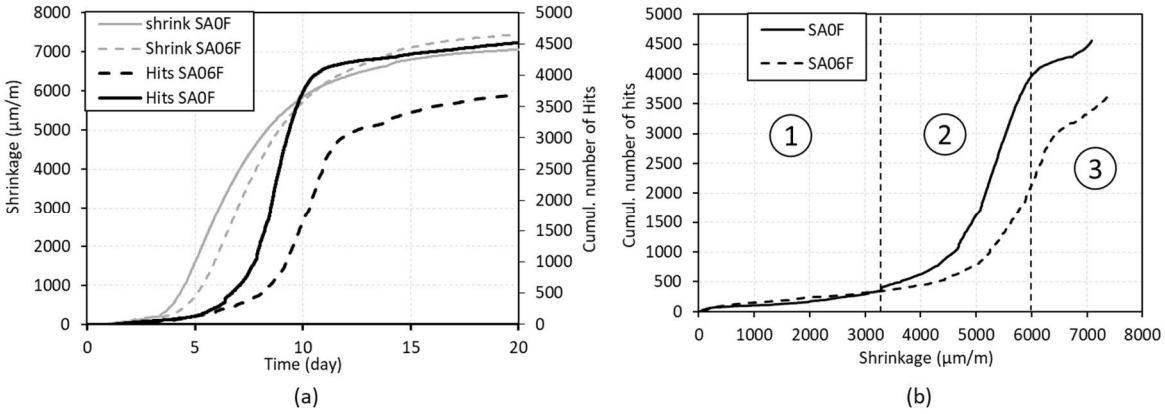

Figure 10. (a) Cumulative number of AE hits in correlation with shrinkage and (b) cumulative number of AE hits in function of shrinkage for SA0F and SA06F.

Several AE parameters have been also studied during drying. **Figure 11** presents the cumulative AE energy in parallel with AE amplitude in function of the time for SA0F and SA06F. AE signals with low energy and low amplitude were generated during the first phase. During the second phase, the cumulative absolute energy increases with an important rate between the 7^{th} and the 11^{th} day after casting indicating an important damage. The amplitude of the detected AE signals increased also and reach a value of 85 dB. In fact, during drying, the water present in the pores of the earth concrete evaporates, inducing suction forces. The negative pressure generated in the pores forces the grains to rearrange and move closer to each other. When the tensile stress is equal to the cohesive force of

attraction between the particles, cracks will be formed [47], [56]. The primary cracks increase in size and new cracks are formed until they intersect. The external surfaces of the earth concrete specimens are more affected because of the strain gradient. In fact, water loss is faster at the surface than inside the specimen according to the drying kinetics which may explain the spalling observed at the surface. During the stabilization phase, the generated AE energy and amplitude decrease quickly indicating a lower degradation rate.

The cumulative absolute energy was more important for mixture with fibers. In addition, this energy liberation appeared later. This could be related to a higher toughness with the addition of fibers. At one hand, micro cracks can initiate at the interface between earth concrete matrix and flax fibers and in the other hand, fibers may be responsible of a different pore size distribution, which can alter drying kinetics, stress redistribution and prevent micro cracks from propagating through the specimen [17,57].

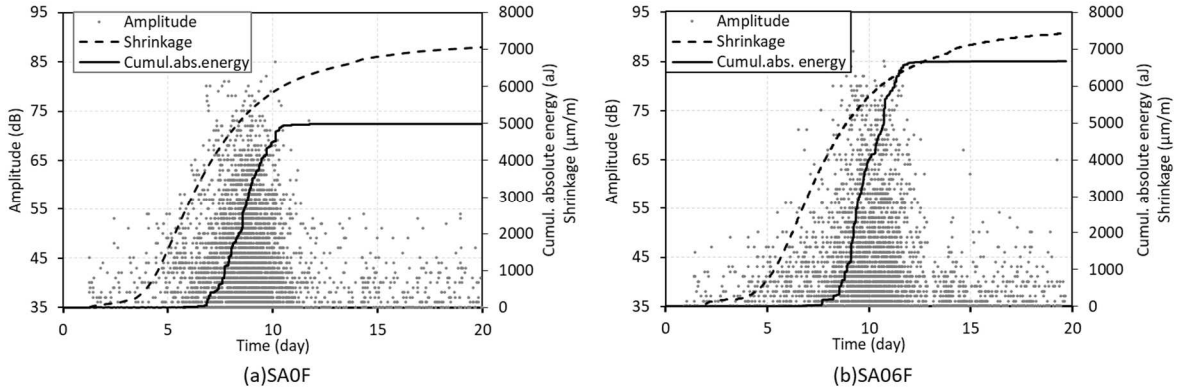

Figure 11. Cumulative AE energy in correlation with AE amplitude and shrinkage in function of time for SA0F and SA06F

4.6 Evolution of Ib-value

The evolution of the micro cracks dimensions, developed during drying, was carried out by measuring the Ib value. The AE peak amplitude is related to the magnitude of the fractures developed during desiccation shrinkage. To determine the overall fracture quantitatively on basis of peak amplitude, the Ib-value originated from seismology is performed. It is defined as the negative gradient

of the seismic magnitude distribution. Statistical values of the amplitude distribution were incorporated to the Ib-value in order to apply it for fracture evaluation in civil engineering materials. According to the cumulative amplitude distribution, the index (Ib-value) changes following the fracture progress [58]. If small-scale fractures are superior to large-scale fractures, Ib-value tend to increase, in the contrary if large-scale fractures are superior to small-scale fractures, Ib-value tends to decrease. Therefore, Ib-value represents the ratio of weak to strong events [59]. Micro-cracks generate a large number of weak acoustic emissions with a high Ib-value. Macro-cracks lead to a relatively low Ib-values since more strong events are generated. The Ib-value was calculated using the peak amplitudes of 100 successive hits, assuming an average amplitude μ and a standard deviation σ of the amplitudes and N the number of hits with an amplitude higher than $\mu - \alpha_1\sigma$ or $\mu - \alpha_2\sigma$ [60]. The formula used to calculate the Ib-value is as follows:

$$Ib = \frac{\log_{10} N(\mu - \alpha_1\sigma) - \log_{10} N(\mu - \alpha_2\sigma)}{(\alpha_1 + \alpha_2)\sigma}$$

where α1 and α2 are constants. α1 and α2 values are 0.5 and 1.5 respectively.

Figure 12 shows the evolution of Ib-value during drying in function of time. Ib-value was important at the beginning and decreased after the 5th day, where damage started to develop with small scale fracturing in the specimen. Ib value attended its minimum stability value after 6 days for SA0F and 8 days for SA06F where the cumulative number of AE hits increased with a high rate. In this phase, micro cracks started to initiate and develop with a larger scale especially near the surface of the specimen where drying is important. Ib value increases again showing stability after 11 days for SA0F and 12 days for SA06F and attend the same value after 14 days. This indicates the presence of two different mechanisms. At the beginning and due to water evaporation, AE hits may be due the retreat of water menisci into the pore. Then, micro cracks initiate and develop with an important rate between the 5th and 12th days after concrete casting generating AE signals with higher amplitude and energy. The third phase indicates a slow propagation of these cracks already developed in the specimen with a lower scale.

Note that, Ib value changes not only in function of the loading level or damage rate but also according to the used concrete, sensors and the applied loading test [35,61].

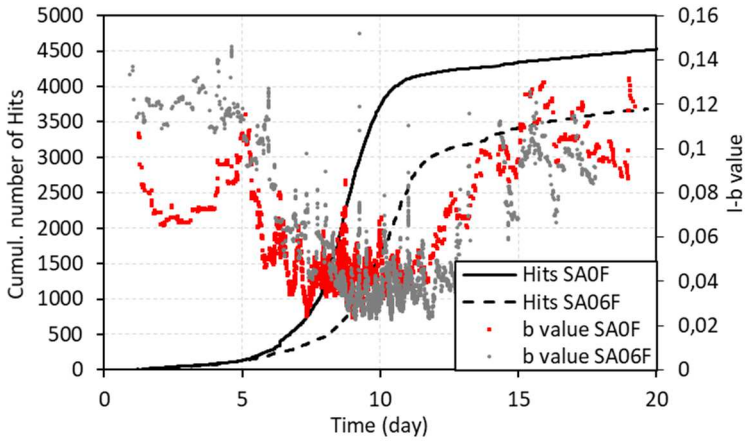

Figure 12. Evolution of Ib-value during drying.

Even though damage evolution was monitored continuously with the AE technique, however the detailed geometry and pattern of the developed cracks are not shown. Additional techniques as the optical microscopy [35], digital image correlation [62], micro-tomography or others could be used to obtain additional information on micro cracking.

5. Conclusions

The effect of drying on the mechanical properties of earth concrete has been studied. Autogenous and desiccation shrinkage of earth concrete in parallel with the mass loss have been also measured. As a part of the investigation, the ultrasound and the AE techniques were applied to monitor the evolution of damage induced by desiccation shrinkage. AE monitoring allowed a temporal development assessment of damage and the process of drying was characterized by following the AE activity and AE parameters. The results show that the AE technique is able to detect low energy processes during shrinkage as well as damage evolution. The relationship between the AE activity and shrinkage is illustrated and the effect of fibers was investigated. The AE results associated with

shrinkage measurements allow to describe qualitatively the drying process and give wealth information on damage evolution. Three different phases were distinguished during drying indicating different mechanisms. Damage increases during the second phase after 6 days of casting indicating the development of self-restraint cracks. This damage may be partly responsible of the strength reduction observed with the compression tests.

Additional studies will be carried out thereafter to better understand the effect of flax fibers on shrinkage by the classification of AE signals and conducting addition tests at the microscopic level for a better characterization of the interface between fibers and earth concrete matrix.

References

[1] N. Kouta, J. Saliba., B. El Oifi, N. Saiyouri, Study of the effect of flax fibers on the fracture behavior of earth concrete by simultaneous application of digital image correlation and acoustic emission, 10th International Conference on Fracture Mechanics of Concrete and Concrete Structures FraMCoS-X, (2019).

[2] H. Van Damme, H. Houben, Earth concrete. Stabilization revisited, Cem. Concr. Res. 114 (2016) 90–102. https://doi.org/10.1016/j.cemconres.2017.02.035.

[3] N. Kouta, J. Saliba, N. Saiyouri, Effect of flax fibers on early age shrinkage and cracking of earth concrete, Constr. Build. Mater. 254 (2020) 119315. https://doi.org/10.1016/j.conbuildmat.2020.119315.

[4] C.S. Tang, B. Shi, C. Liu, W. Bin Suo, L. Gao, Experimental characterization of shrinkage and desiccation cracking in thin clay layer, Appl. Clay Sci. 52 (2011) 69–77. https://doi.org/10.1016/j.clay.2011.01.032.

[5] D.C. Ngo, J. Saliba, N. Saiyouri, Z.M. Sbartaï, Design of a soil concrete as a new building material – Effect of clay and hemp proportions, J. Build. Eng. 32 (2020) 101553. https://doi.org/10.1016/j.jobe.2020.101553.

[6] J. Saliba, E. Rozière, F. Grondin, A. Loukili, Influence of shrinkage-reducing admixtures on plastic and long-term shrinkage, Cem. Concr. Compos. 33 (2011) 209–217.

https://doi.org/10.1016/j.cemconcomp.2010.10.006.

[7] J. Eid, S. Taibi, J.M. Fleureau, M. Hattab, Drying, cracks and shrinkage evolution of a natural silt intended for a new earth building material. Impact of reinforcement, Constr. Build. Mater. 86 (2015) 120–132. https://doi.org/10.1016/j.conbuildmat.2015.03.115.

[8] J.M. Kanema, J. Eid, S. Taibi, Shrinkage of earth concrete amended with recycled aggregates and superplasticizer: Impact on mechanical properties and cracks, Mater. Des. 109 (2016) 378–389. https://doi.org/10.1016/j.matdes.2016.07.025.

[9] P. Walker, R. Keable, J. Martin, V. Maniatidis, Rammed earth: design and construction guidelines, (2005).

[10] P. Woyciechowski, P.L. Narloch, D. Cichocki, Shrinkage characteristics of cement stabilized rammed earth, MATEC Web Conf. 117 (2017). https://doi.org/10.1051/matecconf/201711700178.

[11] P. Walker, Strength, durability and shrinkage characteristics of cement stabilised soil blocks, Cem. Concr. Compos. 17 (1995) 301–310. https://doi.org/10.1016/0958-9465(95)00019-9.

[12] B.V.V. Reddy, K.S. Jagadish, Influence of soil composition on the strength and durability of soil-cement blocks, Ind. Con. J. 69 (1995) 517–526.

[13] P. Walker, T. Stace, Properties of some cement stabilised compressed earth blocks and mortars, Mater. Struct. Constr. 30 (1997) 545–551. https://doi.org/10.1007/bf02486398.

[14] J.M. Kanema, The influence of soil content on the mechanical properties, drying shrinkage and autogenous shrinkage of earth concrete, J. Build. Eng. 13 (2017) 68–76. https://doi.org/10.1016/j.jobe.2017.07.006.

[15] B. Le Runigo, Durabilité du limon de Jossigny traité à la chaux et soumis à différentes sollicitations hydriques : comportement hydraulique, microtextural et mécanique, Thèse Dr. École Cent. Nantes - Fr. (2008) 196.

[16] S. Diamond, E.B. Kinter, Mechanisms of Soil-Lime Stabilization, Highw. Res. Rec. 92 (1965) 83–102. http://onlinepubs.trb.org/onlinepubs/hrr/1965/92/92-006.pdf.

[17] N. Kouta, J. Saliba, N. Saiyouri, Fracture behavior of flax fibers reinforced earth concrete, Eng. Fract. Mech. (2020) 107378. https://doi.org/10.1016/j.engfracmech.2020.107378.

499 [18] T. Sen, J. Reddy, Application of Sisal, Bamboo, Coir and Jute Natural Composites in
500 Structural Upgradation, Japanese J. Anesthesiol. 64 (2015) 1181–1185.
501 [19] A. Laborel-Préneron, J.E. Aubert, C. Magniont, C. Tribout, A. Bertron, Plant aggregates and
502 fibers in earth construction materials: A review, Constr. Build. Mater. 111 (2016) 719–734.
503 https://doi.org/10.1016/j.conbuildmat.2016.02.119.
504 [20] H.R. Kymäläinen, A.M. Sjöberg, Flax and hemp fibres as raw materials for thermal
505 insulations, Build. Environ. 43 (2008) 1261–1269.
506 https://doi.org/10.1016/j.buildenv.2007.03.006.
507 [21] S. Sangma, D.D. Tripura, Experimental study on shrinkage behaviour of earth walling
508 materials with fibers and stabilizer for cob building, Constr. Build. Mater. 256 (2020) 119449.
509 https://doi.org/10.1016/j.conbuildmat.2020.119449.
510 [22] Ş. Yetgin, Ö. ÇAVDAR, A. Çavdar, The effects of the fiber contents on the mechanic
511 properties of the adobes, Constr. Build. Mater. 22 (2008) 222–227.
512 https://doi.org/10.1016/j.conbuildmat.2006.08.022.
513 [23] M. Bouhicha, F. Aouissi, S. Kenai, Performance of composite soil reinforced with barley
514 straw, Cem. Concr. Compos. 27 (2005) 617–621.
515 https://doi.org/10.1016/j.cemconcomp.2004.09.013.
516 [24] K. Ghavami, R.D. Toledo Filho, N.P. Barbosa, Behaviour of composite soil reinforced with
517 natural fibres, Cem. Concr. Compos. 21 (1999) 39–48. https://doi.org/10.1016/S0958-
518 9465(98)00033-X.
519 [25] K. Otsuka, H. Date, Fracture process zone in concrete tension specimen, Eng. Fract. Mech.
520 65 (2000) 111–131.
521 [26] A.K. Das, D. Suthar, C.K.Y. Leung, Machine learning based crack mode classification from
522 unlabeled acoustic emission waveform features, Cem. Concr. Res. 121 (2019) 42–57.
523 https://doi.org/10.1016/j.cemconres.2019.03.001.
524 [27] E. Tsangouri, L. Michels, M. El Kadi, T. Tysmans, D.G. Aggelis, A fundamental
525 investigation of textile reinforced cementitious composites tensile response by Acoustic
526 Emission, Cem. Concr. Res. 123 (2019) 105776.

https://doi.org/10.1016/j.cemconres.2019.105776.

[28] J. Saliba, D. Mezhoud, Monitoring of steel-concrete bond with the acoustic emission technique, Theor. Appl. Fract. Mech. 100 (2019) 416–425. https://doi.org/10.1016/j.tafmec.2019.01.034.

[29] A. Boniface, J. Saliba, Z.M. Sbartaï, N. Ranaivomanana, J.P. Balayssac, Evaluation of the acoustic emission 3D localisation accuracy for the mechanical damage monitoring in concrete, Eng. Fract. Mech. 223 (2020) 106742. https://doi.org/10.1016/j.engfracmech.2019.106742.

[30] B. Assouli, F. Simescu, G. Debicki, H. Idrissi, Detection and identification of concrete cracking during corrosion of reinforced concrete by acoustic emission coupled to the electrochemical techniques, NDT E Int. 38 (2005) 682–689. https://doi.org/10.1016/j.ndteint.2005.04.007.

[31] J. Saliba, A. Loukili, F. Grondin, J.P. Regoin, Identification of damage mechanisms in concrete under high level creep by the acoustic emission technique, Mater. Struct. Constr. 47 (2014) 1041–1053. https://doi.org/10.1617/s11527-013-0113-6.

[32] T. Chotard, A. Quet, A. Ersen, A. Smith, Application of the acoustic emission technique to characterise liquid transfer in a porous ceramic during drying, J. Eur. Ceram. Soc. 26 (2006) 1075–1084. https://doi.org/10.1016/j.jeurceramsoc.2005.01.048.

[33] A.B. Hossain, J. Weiss, The role of specimen geometry and boundary conditions on stress development and cracking in the restrained ring test, Cem. Concr. Res. 36 (2006) 189–199. https://doi.org/10.1016/j.cemconres.2004.06.043.

[34] L. Assi, V. Soltangharaei, R. Anay, P. Ziehl, F. Matta, Unsupervised and supervised pattern recognition of acoustic emission signals during early hydration of Portland cement paste, Cem. Concr. Res. 103 (2018) 216–225. https://doi.org/10.1016/j.cemconres.2017.10.019.

[35] T. Shiotani, J. Bisschop, J.G.M. Van Mier, Temporal and spatial development of drying shrinkage cracking in cement-based materials, Eng. Fract. Mech. 70 (2003) 1509–1525. https://doi.org/10.1016/S0013-7944(02)00150-9.

[36] E.D. Dzaye, G. De Schutter, D.G. Aggelis, Monitoring early-age acoustic emission of cement

555 paste and fly ash paste, Cem. Concr. Res. 129 (2020) 105964.
556 https://doi.org/10.1016/j.cemconres.2019.105964.
557 [37] P. Lura, J. Couch, O.M. Jensen, J. Weiss, Early-age acoustic emission measurements in
558 hydrating cement paste: Evidence for cavitation during solidification due to self-desiccation,
559 Cem. Concr. Res. 39 (2009) 861–867. https://doi.org/10.1016/j.cemconres.2009.06.015.
560 [38] (2015). EN (European Standards), Lime: Definitions, Specifications and Conformity criteria.
561 EN 459-1, No Title, (n.d.).
562 [39] (2012) EN (European Standards), Composition, Specifications and Conformity criteria of
563 common cements. NF EN197-1, No Title, (n.d.).
564 [40] F.G. Bell, Lime stabilization of clay minerals and soils, Eng. Geol. 42 (1996) 223–237.
565 https://doi.org/10.1016/0013-7952(96)00028-2.
566 [41] S.A. Khattab, M. Al-Mukhtar, J.M. Fleureau, Long-term stability characteristics of a lime-
567 treated plastic soil, J. Mater. Civ. Eng. 19 (2007) 358–366.
568 [42] C.A. Anagnostopoulos, Strength properties of an epoxy resin and cement-stabilized silty clay
569 soil, Appl. Clay Sci. 114 (2015) 517–529. https://doi.org/10.1016/j.clay.2015.07.007.
570 [43] J. Page, F. Khadraoui, M. Gomina, M. Boutouil, Influence of different surface treatments on
571 the water absorption capacity of flax fibres : Rheology of fresh reinforced-mortars and
572 mechanical properties in the hardened state, Constr. Build. Mater. 199 (2019) 424–434.
573 https://doi.org/10.1016/j.conbuildmat.2018.12.042.
574 [44] J. Page, F. Khadraoui, M. Boutouil, M. Gomina, Multi-physical properties of a structural
575 concrete incorporating short flax fibers, Constr. Build. Mater. 140 (2017) 344–353.
576 https://doi.org/10.1016/j.conbuildmat.2017.02.124.
577 [45] V. Anggraini, B.B.K. Huat, A. Asadi, H. Nahazanan, Relationship between the compressive
578 and tensile strengths of lime-treated clay containing coconut fibres, Acta Geotech. Slov. 12
579 (2015) 49–57.
580 [46] A.S. Muntohar, A. Widianti, E. Hartono, W. Diana, Engineering properties of silty soil
581 stabilized with lime and rice husk ash and reinforced with waste plastic fiber, J. Mater. Civ.
582 Eng. 25 (2013) 1260–1270. https://doi.org/10.1061/(ASCE)MT.1943-5533.0000659.

583 [47] X. Qiang, L. Hai-jun, L. Zhen-ze, L. Lei, Cracking , water permeability and deformation of
584 compacted clay liners improved by straw fi ber, Eng. Geol. 178 (2014) 82–90.
585 https://doi.org/10.1016/j.enggeo.2014.05.013.
586 [48] C. Barrier, Effects of Fiber Additives on the Desiccation Crack Behavior of the Compacted
587 Akaboku Soil as A Material for Landfill, (2008) 141–149. https://doi.org/10.1007/s11270-
588 008-9703-2.
589 [49] E. Quagliarini, S. Lenci, The influence of natural stabilizers and natural fibres on the
590 mechanical properties of ancient Roman adobe bricks, J. Cult. Herit. 11 (2010) 309–314.
591 https://doi.org/10.1016/j.culher.2009.11.012.
592 [50] G. Srikar, G. Anand, S. Suriya Prakash, A Study on Residual Compression Behavior of
593 Structural Fiber Reinforced Concrete Exposed to Moderate Temperature Using Digital Image
594 Correlation, Int. J. Concr. Struct. Mater. 10 (2016) 75–85. https://doi.org/10.1007/s40069-
595 016-0127-x.
596 [51] G. Ye, P. Lura, K. Van Breugel, A.L.A. Fraaij, Study on the development of the
597 microstructure in cement-based materials by means of numerical simulation and ultrasonic
598 pulse velocity measurement, Cem. Concr. Compos. 26 (2004) 491–497.
599 https://doi.org/10.1016/S0958-9465(03)00081-7.
600 [52] Ş. Erdogdu, U. Kandil, M. Nas, Ş. Kurbetci, S. Nayir, Yüksek Sıcaklığa Maruz Uçucu Kül
601 İçeren Betonun Ultrases Geçiş Hızı ve Basınç Dayanımının Değerlendirilmesi, Nevşehir
602 Bilim ve Teknol. Derg. 6 (2017) 314–325. https://doi.org/10.17100/nevbiltek.322416.
603 [53] E.D. Dzaye, G. De Schutter, D.G. Aggelis, Monitoring early-age acoustic emission of cement
604 paste and fl y ash paste, Cem. Concr. Res. 129 (2020) 105964.
605 https://doi.org/10.1016/j.cemconres.2019.105964.
606 [54] L. Topolář, L. Pazdera, B. Kucharczyková, J. Smutnỳ, K. Mikulášek, Using acoustic emission
607 methods to monitor cement composites during setting and hardening, Appl. Sci. 7 (2017).
608 https://doi.org/10.3390/app7050451.
609 [55] J. Bisschop, J.G.M. Van Mier, How to study drying shrinkage microcracking in cement-based
610 materials using optical and scanning electron microscopy?, Cem. Concr. Res. 32 (2002) 279–

611 287. https://doi.org/10.1016/S0008-8846(01)00671-8.
612 [56] A. Aldaood, M. Bouasker, M. Al-mukhtar, Impact of wetting – drying cycles on the
613 microstructure and mechanical properties of lime-stabilized gypseous soils, Eng. Geol. 174
614 (2014) 11–21. https://doi.org/10.1016/j.enggeo.2014.03.002.
615 [57] B. Kim, W.J. Weiss, Using acoustic emission to quantify damage in restrained fiber-
616 reinforced cement mortars, Cem. Concr. Res. 33 (2003) 207–214.
617 https://doi.org/10.1016/S0008-8846(02)00978-X.
618 [58] D.G. Aggelis, D. V. Soulioti, N. Sapouridis, N.M. Barkoula, A.S. Paipetis, T.E. Matikas,
619 Acoustic emission characterization of the fracture process in fibre reinforced concrete,
620 Constr. Build. Mater. 25 (2011) 4126–4131.
621 https://doi.org/10.1016/j.conbuildmat.2011.04.049.
622 [59] J.H. Kurz, F. Finck, C.U. Grosse, H.W. Reinhardt, Stress drop and stress redistribution in
623 concrete quantified over time by the b-value analysis, Struct Heal. Monit. 5 (2005) 69–81.
624 [60] T. Shiotani, K. Fujii, T. Aoki, K. Amou, Evaluation of progressive failure using AE sources
625 and improved b-value on slope model tests, Prog. Acoust. Emiss VII. 7 (1994) 529–534.
626 [61] D.G. Aggelis, T. Shiotani, S. Momoki, A. Hirama, Acoustic emission and ultrasound for
627 damage characterization of concrete elements, ACI Mater J. 106 (2009) 509–514.
628 [62] F. Lagier, X. Jourdain, C. De Sa, F. Benboudjema, J.B. Colliat, Numerical strategies for
629 prediction of drying cracks in heterogeneous materials : Comparison upon experimental
630 results, 33 (2011) 920–931. https://doi.org/10.1016/j.engstruct.2010.12.013.
631